Single-Molecule Magnets: Tetranuclear Vanadium(III) Complexes with a Butterfly Structure and an $S = 3$ Ground State

Stephanie L. Castro,[1a] Ziming Sun,[1b] Craig M. Grant,[1a] John C. Bollinger,[1a] David N. Hendrickson,*[,1b] and George Christou*[,1a]

Contribution from the Department of Chemistry and Molecular Structure Center, Indiana University, Bloomington, Indiana 47405-4001, and Department of Chemistry-0358, University of California at San Diego, La Jolla, California 92093-0358

Received September 15, 1997

Abstract: Reactions of $VCl_3(THF)_3$, bpy, and NaO_2CR (R = Et, Ph; bpy = 2,2′-bipyridine) in a 1:1:3 ratio in Me_2CO give $[V_4O_2(O_2CR)_7(bpy)_2](ClO_4)$ (R = Et, **1**; R = Ph, **4**) following addition of $NBu^n_4ClO_4$. Use of 4,4′-dimethyl- or 5,5′-dimethylbipyridine (4,4′-Me_2bpy and 5,5′-Me_2bpy, respectively) and R = Et leads similarly to $[V_4O_2(O_2CEt)_7(L-L)_2](ClO_4)$ (L−L = 4,4′-Me_2bpy, **2**; L−L = 5,5′-Me_2bpy, **3**). Yields are in the 38−90% range. The cation of **1** is isostructural with previously prepared $[M_4O_2(O_2CR)_7(bpy)_2]^+$ (M = Cr^{III}, Mn^{III}, Fe^{III}) species and possesses a $[V_4O_2]$ butterfly core. 1D and 2D COSY ^1H NMR spectra of **1** show the solid-state structure is retained on dissolution. The effective magnetic moment (μ_{eff}) per V_4 for **1** gradually rises from 5.79 μ_B at 300 K to a maximum of 6.80 μ_B at 25.0 K and then decreases rapidly to 4.72 μ_B at 2.00 K. The data in the 7.00−300 K range were fit to the appropriate theoretical expression (based on $\hat{H} = -2JS_i \cdot S_j$) to give $J_{bb} = -31.2$ cm^{-1}, $J_{wb} = +27.5$ cm^{-1}, and $g = 1.82$, (b = body, w = wingtip). These values indicate a $S_T = 3$ ground state, confirmed by magnetization vs field studies. Similar results were obtained for the 2-picolinate (pic) analogue of **1** (complex **5**). The $S_T = 3$, 1, 3, and 0 ground states for the $M = V^{III}$, Cr^{III}, Mn^{III}, and Fe^{III}, respectively, are rationalized using spin frustration arguments based on competition between J_{bb} and J_{wb} interactions. AC magnetic susceptibility studies down to 1.7 K on **1** and **5** show weak out-of-phase signals (χ''_M) below 4.0 K and corresponding small decreases in the in-phase signals (χ'_M), indicating that the relaxation of magnetization is unusually slow and comparable with the oscillating AC field (250−1000 Hz). This is a characteristic signature of a single-molecule magnet. Simultaneous application of AC and DC fields has the effect of increasing the barrier to magnetization relaxation, causing the χ''_M signal to move to higher temperature and consequently leading to a much stronger χ''_M signal and, for **5**, the observation of a peak at ∼2.0 K. A dependence of the χ''_M peak position of **5** on the DC field intensity and AC field oscillation frequency is found.

Introduction

Magnetic particles of size < 100 nm are expected to exhibit unusual properties and are therefore the subject of much current interest.[2] Such nanomagnets have been most frequently prepared by fragmenting bulk ferro- or ferrimagnetic materials, but this approach unfortunately suffers from the production of particles with a distribution of sizes, complicating the study of size vs property relationships and precluding a uniform response to an external influence such as an applied magnetic field. Attempts to overcome such problems have included the use of the protein ferritin as a vessel for the synthesis and study of nanoscale magnetic particles.[3]

Exciting developments in the past few years have demonstrated an alternative approach to nanoscale magnets: it has been discovered that certain molecules can function as nanomagnets,[4−27] and such a molecule has been termed a "single-molecule magnet" (SMM).[25] They are prepared by

(1) Indiana University. (b) University of California.

(2) Awschalom, D. D.; Di Vincenzo, D. P. *Physics Today* **1995**, *48*, 43. (b) Leslie-Pelecky, D. L.; Rieke, R. D. *Chem. Mater.* **1996**, *8*, 1770. (c) Gunther, L. *Physics World* **1990**, *December*, 28. (d) Awschalom, D. D.; Di Vincenzo, D. P.; Smyth, J. F. *Science* **1992**, *258*, 414. (e) Stamp, P. C. E.; Chudnosvsky, E. M.; Barbara, B. *Int. J. Mod. Phys.* **1992**, *B6*, 1355.

(3) Gider, S.; Awschalom, D. D.; Douglas, T.; Mann, S.; Chaparala, M. *Science* **1995**, *268*, 77.

(4) Sessoli, R.; Tsai, H.-L.; Schake, A. R.; Wang, S.; Vincent, J. B.; Folting, K.; Gatteschi, D.; Christou, G.; Hendrickson, D. N. *J. Am. Chem. Soc.* **1993**, *115*, 1804. (b) Sessoli, R.; Gatteschi, D.; Caneschi, A.; Novak, M. A. *Nature* **1993**, *365*, 141.

(5) Villain, J.; Hartman-Boutron, F.; Sessoli, R.; Rettori, A. *Europhys. Lett.* **1994**, *27*, 159.

(6) Eppley, H. J.; Tsai, H.-L.; De Vries, N.; Folting, K.; Christou, G.; Hendrickson, D. N. *J. Am. Chem. Soc.* **1995**, *117*, 301.

(7) Novak, M. A.; Sessoli, R.; Caneschi, A.; Gatteschi, D. *J. Magn. Magn. Mater.* **1995**, *146*, 211.

(8) Barbara, B.; Wernsdorfer, W.; Sampaio, L. C.; Park, J. G.; Paulsen, C.; Novak, M. A.; Ferré, R.; Mailly, D.; Sessoli, R.; Caneschi, A.; Hasselbach, K.; Benoit, A.; Thomas, L. *J. Magn. Magn. Mater.* **1995**, *140−144*, 1825.

(9) Tsai, H.-L.; Eppley, H. J.; De Vries, N.; Folting, K.; Christou, G.; Hendrickson, D. N. *Mol. Cryst. Liq. Cryst.* **1995**, *274*, 167.

(10) Novak, M. A.; Sessoli, R. In *Quantum Tunneling of Magnetization − QTM '94*; Kluwer Academic Publishers: Dordrecht, 1995; pp 171−188.

(11) Paulsen, C.; Park, J.-G. In *Quantum Tunneling of Magnetization − QTM '94*; Gunther, L., Barbara, B., Eds.; Kluwer Academic Publishers: Dordrecht, 1995; pp 189−207.

(12) Paulsen, C.; Park, J.-G.; Barbara, B.; Sessoli, R.; Caneschi, A. *J. Magn. Magn. Mater.* **1995**, *140−144*, 379 and 181.

(13) Friedman, J. R.; Sarachik, M. P.; Tejada, J.; Maciejewski, J.; Ziolo, R. *J. Appl. Phys.* **1996**, *79*, 6031. (b) Friedman, J. R.; Sarachik, M. P.; Tejada, J.; Ziolo, R. *Phys. Rev. Lett.* **1996**, *76*, 3830.

(14) Thomas, L.; Lionti, F.; Ballou, R.; Gatteschi, D.; Sessoli, R.; Barbara, B. *Nature* **1996**, *383*, 145.

(15) Tejada, J.; Ziolo, R. F.; Zhang, X. X. *Chem. Mater.* **1996**, *8*, 1784.

S0002-7863(97)03243-5 CCC: $15.00
Published on Web 02/27/1998

solution methods from simple reagents and, being readily purified, are composed of discrete molecular units of a single, sharply defined size. Unlike normal magnets, whose properties are the result of interactions between large numbers of individual spin carriers within domains in crystals, the behavior of a SMM arises from the intrinsic properties of individual molecules, i.e., no intermolecular interactions are required. Single-molecule magnets are magnetizable magnets: in an external magnetic field, their magnetic moments can all be oriented either "up" or "down", and when the external field is removed, the moments (spins) of the molecules will reorient only very slowly if the temperature is low enough, i.e., the magnetization is retained in zero field. A SMM is thus magnetizable because there is a big enough potential energy barrier between its spin "up" and "down" states. There are two requirements for this: (i) the SMM must have a relatively large spin (S) ground state, and (ii) there has to be a large and negative magnetic anisotropy, arising from zero-field splitting ($H = DS_z^2$) in the ground state with $D < 0$. Both these requirements are necessary because the potential energy barrier is $S^2|D|$ for integer S and $(S^2\text{-}^1/_4)|D|$ for half-integer spin.

The most thoroughly studied example of a SMM is $[Mn_{12}O_{12}(O_2CMe)_{16}(H_2O)_4]\cdot 2MeCO_2H\cdot 4H_2O$ with $S = 10$.[4−23,28] The related complexes $[Mn_{12}O_{12}(O_2CR)_{16}(H_2O)_x]$ (R = Et, x = 3;[6] R = Ph, x = 4[6]) with S = 9 or 10 also show SMM properties, as does $(PPh_4)[Mn_{12}O_{12}(O_2CEt)_{16}(H_2O)_4]$, the first ionic SMM.[6,29,30] More recently, a second class of SMM has been discovered, the family of Mn molecules of formulation $[Mn_4O_3X(O_2CMe)_3(dbm)_3]$ (X = various; dbm^- = the anion of dibenzoylmethane) with a $[Mn_4(\mu_3\text{-}O)_3(\mu_3\text{-}X)]^{6+}$ highly distorted cubane core and an S = 9/2 ground state.[24−26] Additionally, $[Fe_8O_2(OH)_{12}(tacn)_6]^{8+}$ (tacn = 1,4,7-triazacyclononane) has been reported to exhibit SMM behavior.[27]

The SMM field is now established and among the many challenges for the future is the synthesis of new members of this class to help expand our knowledge of this phenomenon. This is particularly important given (i) the potential of nanomagnets comprising single molecules to provide the ultimate high-density memory device and (ii) the ability to use such species to study how quantum mechanical behavior at the macroscopic scale underlies classical behavior at the macroscopic scale, given that for nanomagnets it is possible to observe macroscopic quantum tunneling of magnetization, as demonstrated for both the $[Mn_{12}O_{12}(O_2CR)_{16}(H_2O)_4]^{0,-}$ [13−15,30] and $[Mn_4O_3Cl(O_2CMe)_3(dbm)_3]$[26] species. In the present work, we report that a new class of V^{III}_4 complexes has been synthesized and fully characterized and that representative examples have been identified as the first examples of a SMM outside Mn and Fe chemistry. The complexes $[V_4O_2(O_2CR)_7(bpy)_2](ClO_4)$ (bpy = 2,2′-bipyridine) and $(NEt_4)[V_4O_2(O_2CEt)_7(pic)_2]$ (pic = 2-picolinate) have been found to exhibit the out-of-phase AC magnetic susceptibility signals diagnostic of a SMM. Some portions of this work have been previously communicated.[31]

Experimental Section

All manipulations were performed under anaerobic conditions using an inert-atmosphere glovebox and a vacuum line in conjunction with standard Schlenk glassware. All solvents were distilled from appropriate drying agents unless otherwise indicated. Solvents were degassed by vacuum/nitrogen cycles. $VCl_3(THF)_3$ was prepared as described in the literature.[32] "$[Cr_3(OH)_2(O_2CMe)_7]$", 2,2′-bipyridine, and 4,4′-dimethyl-2,2′-bipyridine (4,4′-Me_2bpy) were used as received (Aldrich). 5,5′-Dimethyl-2,2′-bipyridine (5,5′-Me_2bpy) was prepared by a literature procedure.[33] $NBu^n_4ClO_4$ was prepared by neutralization of a 40% w/w solution of NBu^n_4OH in H_2O (Aldrich) with $HClO_4$ (conc). The resulting white precipitate was recrystallized from CH_2Cl_2/Et_2O and dried in vacuo at room temperature. Sodium propionate and benzoate were prepared by adding elemental sodium to a slight excess of the carboxylic acid in THF; the resulting white solids were collected by filtration, washed copiously with Et_2O, and dried in vacuo.

$[V_4O_2(O_2CEt)_7(bpy)_2](ClO_4)$ (1). A reaction slurry consisting of $VCl_3(THF)_3$ (1.12 g, 3.00 mmol), bpy (0.468 g, 3.00 mmol), and NaO_2-CEt (0.829 g, 9.00 mmol) in acetone (50 mL; degassed but not distilled) was stirred overnight at room temperature to give a red-brown solution and an off-white precipitate of NaCl. The latter was removed by filtration, and $NBu^n_4ClO_4$ (0.26 g, 0.75 mmol) was added to the filtrate. The solvent was then removed in vacuo, and the resulting red-brown oil was washed with Et_2O (3 × 50 mL) and redissolved in acetone (10 mL; distilled from 4A molecular sieves). Addition of a large excess of Et_2O precipitated a brown microcrystalline precipitate which was collected by filtration, was washed with Et_2O, and dried in vacuo; the yield was 70−90%. Anal. Calcd (found) for $\mathbf{1}\cdot Et_2O\cdot H_2O$ ($C_{45}H_{63}N_4O_{22}ClV_4$): C, 43.20 (43.29); H, 5.08 (5.12); N, 4.48 (4.29). Electronic spectrum in CH_2Cl_2: λ_{max}, nm (ϵ_M, L mol^{-1} cm^{-1}); 214 (38 200), 246 (29 600), 300 (29 100), 488 (2450), 678 (920). Selected IR data (cm^{-1}, Nujol): 1583 (s), 1495 (m), 1300 (s), 1219 (m), 1174 (w), 1161 (w), 1080 (s), 1028 (s), 962 (w), 812 (m), 779 (s), 736 (s), 682 (s), 652 (s), 638 (s), 623 (m), 576 (m), 422 (s).

$[V_4O_2(O_2CEt)_7(4,4'\text{-}Me_2bpy)_2](ClO_4)$ (2). This complex was made by substituting 4,4′-dimethyl-2,2′-bipyridine (4,4′-Me_2bpy) for bpy in the procedure for complex **1**. The product was obtained in 46% yield. The same procedure but with 5,5′-Me_2bpy gave $[V_4O_2(O_2CEt)_7(5,5'\text{-}Me_2bpy)_2](ClO_4)$ (**3**) in 38% yield. Complexes **2** and **3** were pure by ^{1}H NMR spectroscopy.

$[V_4O_2(O_2CPh)_7(bpy)_2](ClO_4)$ (4). This complex was made by substituting NaO_2CPh for NaO_2CEt in the procedure for complex **1**. The product was obtained in 47% yield. Anal. Calcd (found) for **4** ($C_{69}H_{56}N_4O_{20}ClV_4$): C, 55.4 (55.32); H, 3.4 (3.50); N, 3.7 (3.73).

$[NEt_4][V_4O_2(O_2CEt)_7(pic)_2]$ (5). To a stirred mixture of $VCl_3(THF)_3$ (0.747 g, 2.00 mmol) and NaO_2CEt (0.552 g, 6.00 mmol) in MeCN (20 mL) was added Na(pic) (0.145 g, 1.00 mmol) dissolved in H_2O (250 μL). The mixture was stirred overnight to give a dark green solution and an off-white precipitate (NaCl). The solution was filtered,

(16) Hernandez, J. M.; Zhang, X. X.; Luis, F.; Bartolomé, J.; Tejada, J.; Ziolo, R. *Europhys. Lett.* **1996**, *35*, 301.
(17) Chudnovsky, E. M. *Science* **1996**, *274*, 938.
(18) Lionti, F.; Thomas, L.; Ballou, R.; Barbara, B.; Sulpice, A.; Sessoli, R.; Gatteschi, D. *J. Appl. Phys.* **1997**, *81*, 4608.
(19) Friedman, J. R.; Sarachik, M. P.; Hernandez, J. M.; Zhang, X. X.; Tejada, J.; Molins, E.; Ziolo, R. *J. Appl. Phys.* **1997**, *81*, 3978.
(20) Aubin, S. M. J.; Spagna, S.; Eppley, H. J.; Sager, R. E.; Folting, K.; Christou, G.; Hendrickson, D. N. *Mol. Cryst. Liq. Cryst.*, in press.
(21) Eppley, H. J.; Aubin, S. M. J.; Wemple, M. W.; Adams, D. M.; Tsai, H.-L.; Grillo, V. A.; Castro, S. L.; Sun, Z.; Folting, K.; Huffman, J. C.; Hendrickson, D. N.; Christou, G. *Mol. Cryst. Liq. Cryst.*, in press.
(22) Luis, F.; Bartolomé, J.; Fernandez, J. F. *Phys. Rev. B* **1997**, *55*, 11448.
(23) Hernandez, J. M.; Zhang, X. X.; Luis, F.; Tejada, J.; Friedman, J. R.; Sarachik, M. P.; Ziolo, R. *Phys. Rev. B* **1997**, *55*, 5858.
(24) Wemple, M. W.; Adams, D. M.; Hagen, K. S.; Folting, K.; Hendrickson, D. N.; Christou, G. *J. Chem. Soc., Chem. Commun.* **1995**, 1591.
(25) Aubin, S. M. J.; Wemple, M. W.; Adams, D. M.; Tsai, H.-L.; Christou, G.; Hendrickson, D. N. *J. Am. Chem. Soc.* **1996**, *118*, 7746.
(26) Aubin, S. M. J.; Dilley, N. R.; Wemple, M. W.; Maple, M. B.; Christou, G.; Hendrickson, D. N., submitted for publication.
(27) Barra, A. L.; Debrunner, P.; Gatteschi, D.; Schultz, C. E.; Sessoli, R. *Europhys. Lett.* **1996**, *35*, 133.
(28) Lis, T. *Acta Crystallogr.* **1980**, *B36*, 2042.
(29) Schake, A. R.; Tsai, H.-L.; De Vries, N.; Webb, R. J.; Folting, K.; Hendrickson, D. N.; Christou, G. *J. Chem. Soc., Chem. Commun.* **1992**, 181.
(30) Aubin, S. M. J.; Spagna, S.; Eppley, H. J.; Sager, R. E.; Christou, G.; Hendrickson, D. N. *Chem. Commun.* In press.
(31) Castro, S. L.; Sun, Z.; Bollinger, J. D.; Hendrickson, D. N.; Christou, G. *J. Chem. Soc., Chem. Commun.* **1995**, 2517.
(32) Manzer, L. E. *Inorg. Synth.* **1982**, *21*, 138.
(33) Ebmeyer, F.; Vögtle, F. *Chem. Ber.* **1989**, *122*, 1725. (b) Badger, G. M.; Sasse, W. H. F. *J. Chem. Soc.* **1956**, 616. (c) Sasse, W. H. F.; Whittle, C. P. *J. Chem. Soc.* **1961**, 1347.

Table 1. Crystallographic Data for Complex **1**·$2CH_2Cl_2$

formula	$C_{43}H_{55}Cl_5N_4O_{20}V_4$	fw[a]	1328.95 g·mol^{-1}
a =	13.302(3) Å	space group	$P\bar{1}$
b =	13.265(3) Å	T =	−161 °C
c =	15.905(4) Å	λ =	0.710 69 Å
α =	87.51(1)°	D_{calc} =	1.588 g cm^{-3}
β =	96.70(1)°	μ =	9.459 cm^{-1}
γ =	86.66(1)°	$R(F_o)$[c] =	0.0716
V =	2778.8 Å^3	$R_w(F_o)$[d]	0.1649
Z =	2		

[a] Including solvate molecules. [b] Graphite monochromator. [c] $R = \sum||F_o| - |F_c||/\sum|F_o|$. [d] $R_w = [\sum w(|F_o| - |F_c|)^2/\sum w|F_o|^2]^{1/2}$ where $w = 1/\sigma^2(|F_o|)$.

and NEt_4Cl (0.083 g, 0.50 mmol) was added to the filtrate. The MeCN was removed in vacuo, and the remaining green oil redissolved in anhydrous acetone (10 mL). THF (10 mL) was added, and the green solution was left undisturbed at room temperature. After a few days, a green-black microcrystalline solid had precipitated, and this was collected by filtration, washed with THF (10 mL), and dried in vacuo. The yield was 53%. Anal. Calcd (found) for $C_{41}H_{63}N_3O_{20}V_4$: C, 43.90 (43.20); H, 5.66 (5.49); N, 3.75 (3.64)%. Selected IR data (cm^{-1}, Nujol): 1664 (s), 1593 (s, br), 1342 (s), 1294 (s), 1242 (m), 1184 (2), 1167 (m), 1082 (m), 1049 (m), 1026 (w), 1010 (m), 885 (w), 854 (m), 810 (m), 773 (m), 707 (m), 698 (m), 540 (m, br), 416 (s) cm^{-1}.

$[Cr_4O_2(O_2CMe)_7(bpy)_2](ClO_4)$ (6). This complex was prepared by a modification to the procedure of Vincent and co-workers.[34] A green slurry of "$Cr_3(OH)_2(O_2CMe)_7$" (1.81 g, 3.00 mmol), bpy (1.41 g, 9.00 mmol), and $NBu^n_4ClO_4$ (1.03 g, 3.00 mmol) in PhCN (60 mL) was maintained at reflux for 3.5 h. The purple solution was cooled, and Et_2O (∼100 mL) was added to precipitate a solid. The solid was collected by filtration, washed with Et_2O, and recrystallized from a CH_2Cl_2/hexanes layering. The product was rather oily, and it was separated by decantation, washed with hexanes, and dried in vacuo to give a free-flowing microcrystalline purple solid. The yield was 33%. The solid appears hygroscopic and was stored in a glovebox. Anal. Calcd (found) for **6**·$^1/_2Et_2O$ ($C_{36}H_{42}N_4O_{20.5}ClCr_4$): C, 39.23 (39.67); H, 3.84 (3.65); N, 5.08 (4.94).

X-ray Crystallography. Crystals suitable for crystallography were grown from a CH_2Cl_2/hexanes layering, and these were subsequently identified crystallographically as **1**·$2CH_2Cl_2$. A suitable single crystal was chosen from the bulk sample and affixed to the tip of a glass fiber with silicone grease. The mounted sample was transferred to the goniostat and cooled to −161 °C for characterization and data collection. The equipment employed was a Picker four-circle diffractometer; details of the diffractometry, low-temperature facilities, and computational procedures employed by the Molecular Structure Center are available elsewhere.[35] A systematic search of a limited hemisphere of reciprocal space located a set of intensities with no Laue symmetry or systematic absences, indicting a triclinic space group. Subsequent solution and refinement of the structure confirmed the choice of the centrosymmetric space group $P\bar{1}$. After data collection ($6° \leq 2\theta \leq 45°$; $+h,\pm k,\pm l$), the intensities were corrected for Lorentz and polarization effects, and equivalent data were averaged (R for averaging = 0.040). The structure was solved by direct methods (SHELXTL) and Fourier techniques. All non-hydrogen atoms, including those of two well-behaved CH_2Cl_2 solvate molecules, were refined with anisotropic thermal parameters. Hydrogen atoms were located in a difference Fourier map phased on the non-hydrogen atoms and included in the final least-squares refinement cycles with isotropic thermal parameters. A final difference Fourier map was essentially featureless, with the largest peak having an intensity of 1.46 e/Å.^{3} Crystallographic data are summarized in Table 1.

Physical Measurements. ^{1}H NMR spectra were collected on a 300 MHz Varian Gemini 2000 spectrometer with the protio-solvent signal used as reference. IR and electronic spectra were recorded on Nujol mulls and solutions, respectively, on Nicolet Model 510P and Hewlett Packard Model 8452A spectrophotometers, respectively. DC magnetic susceptibility data were collected on powdered, microcrystalline samples (restrained in Vaseline to prevent torquing) on a Quantum Design MPMS5 SQUID magnetometer equipped with a 5.5 T (55 kG) magnet. A diamagnetic correction to the observed susceptibilities was applied using Pascal's constants. AC magnetic susceptibility measurements were made on a Quantum Design MPMS2 SQUID magnetometer equipped with a 1 T (10 kG) magnet and capable of achieving temperatures of 1.7−400 K. The AC field range is 1×10^{-4}−5 G oscillating at a frequency in the range 5×10^{-4}−1512 Hz. AC susceptibility data were collected on powdered, microcrystalline samples in an AC field of 1.0 G oscillating in the 250−1000 Hz and in an applied DC field of 0−8.0 kG.

Results

Syntheses. The possibility for the preparation of $[V_4O_2(O_2CR)_7(bpy)_2]^+$ salts was originally suggested by the fact that $[M_4O_2(O_2CR)_7(bpy)_2](ClO_4)$ complexes were already known for M = Cr^{III} (**6**),[34,36] Mn^{III} (**7**),[37] and Fe^{III} (**8**),[38] and there seemed no reason to believe that the M = V^{III} analogues should not also be accessible if the right procedure could be developed. After some preliminary experimentation, a successful procedure was indeed devised. Treatment of $VCl_3(THF)_3$, bpy, and NaO_2CEt in a 1:1:3 molar ratio in Me_2CO led to isolation of $[V_4O_2(O_2CEt)_7(bpy)_2](ClO_4)$ (**1**) after addition of ClO_4^-. The oxide ion most likely arises from solvent H_2O impurities (thus, to optimize yield, the solvent was degassed but not dried), and the preparation may be summarized as in eq 1. The 2-fold

$$4VCl_3 + 2bpy + 11NaO_2CEt + 2H_2O \rightarrow [V_4O_2(O_2CEt)_7(bpy)_2]^+ + 4EtCO_2H + Cl^- + 11NaCl \quad (1)$$

excess of bpy over that required by eq 1 was found to be beneficial in providing high yields of product, although the reason for this is not clear. A similar bpy effect has been noted previously.[39] The reaction can readily be altered with respect to the identities of the carboxylate and the chelate, as confirmed by the preparation of the 4,4′-Me_2bpy (**2**) and 5,5′-Me_2bpy (**3**) derivatives, and the $PhCO_2^-$ derivative (**4**). No doubt the same procedure could also be extended to a number of other carboxylate and substituted-bpy (and phen) groups. In addition, anionic chelates may be incorporated. Thus, use of Na(pic) (pic^- = picolinate) leads to the formation of $(NEt_4)[V_4O_2(O_2CEt)_7(pic)_2]$ (**5**), the V^{III}_4 analogue of $(NEt_4)[Mn_4O_2(O_2CR)_7(pic)_2]$ reported several years ago.[40]

Description of Structure. A labeled ORTEP plot of the anion of **1** is shown in Figure 1, and interatomic distances and angles are collected in Table 2. Complex **1**·$2CH_2Cl_2$ crystallizes in the triclinic space group $P\bar{1}$ with the asymmetric unit containing the entire cation, one anion, and two lattice CH_2Cl_2 molecules. The cation contains a $[V_4(\mu_3\text{-}O)_2]^{8+}$ core comprising four V^{III} ions with a "butterfly" disposition and a μ_3-O^{2-} ion bridging each V_3 "wing"; both the oxide ions, O(5) and O(6), lie slightly out of their respective V_3 planes, by 0.328 and 0.317 Å, respectively. Peripheral ligation is provided by seven $EtCO_2^-$ and two bpy chelate groups, the former in their common *syn,syn*-bridging modes and the latter attached to the wingtip

(34) Ellis, T.; Glass, M.; Harton, A.; Folting, K.; Huffman, J. C.; Vincent, J. B. *Inorg. Chem.* **1994**, *33*, 5522.

(35) Chisholm, M. H.; Folting, K.; Huffman, J. C.; Kirkpatrick, C. C. *Inorg. Chem.* **1984**, *23*, 1021.

(36) Bino, A.; Chayat, R.; Pedersen, E.; Schneider, A. *Inorg. Chem.* **1991**, *30*, 856.

(37) Vincent, J. B.; Christmas, C.; Chang, H.-R.; Li, Q.; Boyd, P. D. W.; Huffman, J. C.; Hendrickson, D. N.; Christou, G. *J. Am. Chem. Soc.* **1989**, *111*, 2086.

(38) McCusker, J. K.; Vincent, J. B.; Schmitt, E. A.; Mino, M. L.; Shin, K.; Coggin, D. K.; Hagen, P. M.; Huffman, J. C.; Christou, G.; Hendrickson, D. N. *J. Am. Chem. Soc.* **1991**, *113*, 3012.

(39) Castro, S. L.; Martin, J. D.; Christou, G. *Inorg. Chem.* **1993**, *32*, 2978.

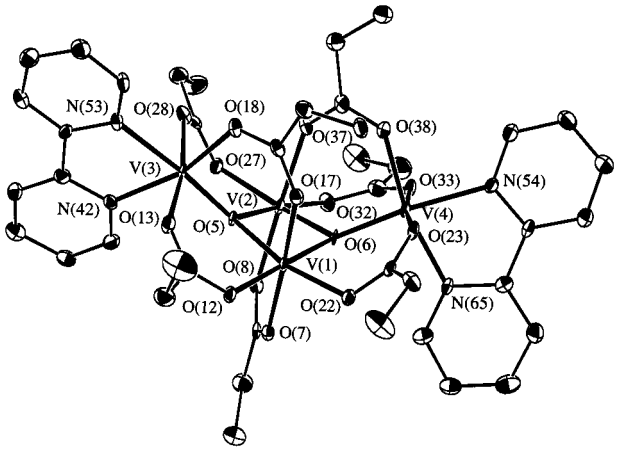

Figure 1. ORTEP representation of the $[V_4O_2(O_2CEt)_7(bpy)_2]^+$ cation of **1** at the 50% probability level.

Table 2. Selected Interatomic Distances (Å) and Angles (deg) for Complex **1**·$2CH_2Cl_2$

V(1)−V(2)	2.909(2)	V(2)−O(5)	1.981(5)	V(3)−O(13)	2.053(5)
V(1)−V(3)	3.315(2)	V(2)−O(32)	1.995(5)	V(3)−N(42)	2.126(5)
V(1)−V(4)	3.480(2)	V(2)−O(27)	2.019(5)	V(3)−N(53)	2.173(6)
V(1)−O(5)	1.928(4)	V(2)−O(8)	2.024(4)	V(4)−O(6)	1.841(4)
V(1)−O(6)	1.972(5)	V(2)−O(37)	2.055(4)	V(4)−O(38)	1.993(5)
V(1)−O(12)	1.988(5)	V(2)−V(4)	3.321(2)	V(4)−O(33)	2.042(5)
V(1)−O(22)	2.004(4)	V(2)−V(3)	3.465(2)	V(4)−O(23)	2.050(5)
V(1)−O(7)	2.053(4)	V(3)−O(5)	1.830(4)	V(4)−N(65)	2.116(6)
V(1)−O(17)	2.085(4)	V(3)−O(18)	1.981(4)	V(4)−N(54)	2.159(6)
V(2)−O(6)	1.931(4)	V(3)−O(28)	2.049(5)		

O(5)−V(1)−O(6)	82.6(2)	O(5)−V(3)−O(13)	95.1(2)
O(5)−V(1)−O(12)	95.9(2)	O(18)−V(3)−O(13)	89.5(2)
O(6)−V(1)−O(12)	176.0(2)	O(28)−V(3)−O(13)	170.5(2)
O(5)−V(1)−O(22)	167.1(2)	O(5)−V(3)−N(42)	99.2(2)
O(6)−V(1)−O(22)	87.6(2)	O(18)−V(3)−N(42)	163.9(2)
O(12)−V(1)−O(22)	94.4(2)	O(28)−V(3)−N(42)	83.4(2)
O(5)−V(1)−O(7)	91.1(2)	O(13)−V(3)−N(42)	91.0(2)
O(6)−V(1)−O(7)	87.1(2)	O(5)−V(3)−N(53)	174.4(2)
O(12)−V(1)−O(7)	89.2(2)	O(18)−V(3)−N(53)	88.7(2)
O(22)−V(1)−O(7)	96.8(2)	O(28)−V(3)−N(53)	86.7(2)
O(5)−V(1)−O(17)	89.1(2)	O(13)−V(3)−N(53)	84.3(2)
O(6)−V(1)−O(17)	96.0(2)	N(42)−V(3)−N(53)	75.3(2)
O(12)−V(1)−O(17)	87.7(2)	O(6)−V(4)−O(38)	95.4(2)
O(22)−V(1)−O(17)	83.6(2)	O(6)−V(4)−O(33)	95.0(2)
O(7)−V(1)−O(17)	176.8(2)	O(38)−V(4)−O(33)	89.2(2)
O(6)−V(2)−O(5)	82.3(2)	O(6)−V(4)−O(23)	93.0(2)
O(6)−V(2)−O(32)	96.3(2)	O(38)−V(4)−O(23)	93.2(2)
O(5)−V(2)−O(32)	174.8(2)	O(33)−V(4)−O(23)	171.4(2)
O(6)−V(2)−O(27)	167.4(2)	O(6)−V(4)−N(65)	98.0(2)
O(5)−V(2)−O(27)	87.8(2)	O(38)−V(4)−N(65)	166.4(2)
O(32)−V(2)−O(27)	94.2(2)	O(33)−V(4)−N(65)	91.6(2)
O(6)−V(2)−O(8)	91.3(2)	O(23)−V(4)−N(65)	84.1(2)
O(5)−V(2)−O(8)	86.6(2)	O(6)−V(4)−N(54)	173.7(2)
O(32)−V(2)−O(8)	88.5(2)	O(38)−V(4)−N(54)	90.8(2)
O(27)−V(2)−O(8)	95.7(2)	O(33)−V(4)−N(54)	83.9(2)
O(6)−V(2)−O(37)	89.6(2)	O(23)−V(4)−N(54)	87.8(2)
O(5)−V(2)−O(37)	97.0(2)	N(65)−V(4)−N(54)	75.8(2)
O(32)−V(2)−O(37)	87.9(2)	V(3)−O(5)−V(1)	123.8(2)
O(27)−V(2)−O(37)	84.0(2)	V(3)−O(5)−V(2)	130.8(2)
O(8)−V(2)−O(37)	176.4(2)	V(1)−O(5)−V(2)	96.2(2)
O(5)−V(3)−O(18)	96.8(2)	V(4)−O(6)−V(2)	123.4(2)
O(5)−V(3)−O(28)	93.5(2)	V(4)−O(6)−V(1)	131.6(2)
O(18)−V(3)−O(28)	93.8(2)	V(2)−O(6)−V(1)	96.4(2)

V^{III} centers, V(3) and V(4). The metals are all octahedrally coordinated, and the entire cation has virtual C_2 symmetry but C_1 crystallographic symmetry. The V···V separations fall into three types: the body/body separation, V(1)···V(2), is short (2.909(2) Å) relative to the wingtip/body separations, which themselves separate into two types, those bridged by two $EtCO_2^-$ groups (V(1)··V(3), 3.315(2); V(2)··V(4), 3.321(2) Å), and those bridged by one (V(1)··V(4), 3.480(2); V(2)··V(3), 3.465(2) Å). The dihedral angle θ between the two V_3 least-squares planes is 133.1°.

Table 3. Comparison of Selected Structural Parameters (Å, deg)[a,b] for the $[M_4O_2(O_2CR)_7(bpy)_2]^+$ Cations of Complexes **1** and **6**−**8**

parameter[c]	V(**1**)	Cr(**6**)	Mn(**7**)	Fe(**8**)
M_b··M_b	2.909(2)	2.784(1)	2.848(5)	2.855(4)
M_b··M_w[b,d]	3.318(2)	3.3163(9)	3.306(5)	3.306(4)
M_b··M_w[b,e]	3.473(2)	3.4274(8)	3.378(5)	3.439(4)
M_b-O_t[b,d]	1.930(4)	1.891(3)	1.903(15)	1.926(5)
M_b-O_t[b,e]	1.977(5)	1.914(2)	1.920(15)	1.947(5)
M_w-O_t	1.842(4)	1.852(3)	1.824(16)	1.819(5)
$M_b-O_t-M_b$[b]	96.3(2)	94.0(1)	96.3(7)	95.0(2)
$M_b-O_t-M_w$[b,d]	123.6(2)	124.8(1)	123.7(8)	123.9(3)
$M_b-O_t-M_w$[b,e]	131.2(2)	131.0(1)	130.2(7)	131.9(3)
θ (dihedral)[f]	133.1	143.0	135.4	139.6
Δ[g]	0.323	0.338	0.334	0.323

[a] Averaged using C_2 virtual symmetry. [b] Quoted esd's for averaged values are the esd's of the individual values. [c] Subscripts: b = body, w = wingtip, t = triply-bridging. [d] For M atoms bridged by two RCO_2^- groups. [e] For M atoms bridged by one RCO_2^- group. [f] Dihedral angle between two M_3 least-squares planes. [g] Distance of O_t to M_3 least-squares plane.

As stated earlier, the cation of **1** is the fourth member of the isostructural $[M_4O_2(O_2CR)_7(bpy)_2]^+$ (M = Fe^{III}, Mn^{III}, Cr^{III}) family of complexes, and it is thus pertinent to ask whether there are any significant structural trends or differences across this series. In Table 3 are compared selected structural parameters for the four complexes, i.e., **1** and **6**−**8**. It is readily apparent that the complexes are essentially isometric, the main variations being between some of the values for the Cr^{III} complex compared with the others; for example, the Cr_b··Cr_b distance appears short, but this is undoubtedly due to the variation in M^{3+} size as gauged by ionic radii[41] values of 0.640 (V^{3+}), 0.615 (Cr^{3+}), 0.645 (Mn^{3+}), and 0.645 (Fe^{3+}) Å, reflecting population of σ-antibonding d-orbitals for high-spin Mn^{3+} and Fe^{3+}. The decreased M_b···M_b separation for Cr^{3+} then also affects the M_b··O_t and $M_b-O_t-M_b$ values. Note also that the Jahn−Teller distortion for high-spin Mn^{3+} complicates close comparisons involving complex **7**. In general, the four complexes are very similar and may be quite satisfactorily described as isostructural.

NMR Spectroscopy. ^1H and ^2H NMR spectroscopy has proven useful in the past for studying complexes **6**−**8** in solution,[37−39] including assessing whether the solid-state structures are retained on dissolution, and complementary studies have therefore been performed with the present complexes. This knowledge will also be of use in future reactivity studies of these molecules. The ^1H NMR spectrum of complex **1** in CD_2Cl_2 is shown in Figure 2, and pertinent data for complexes **1**−**3** are collected in Table 4. Peak assignments were made by consideration of peak integrations, T_1 values, the effect of Me substitution at the bpy 4 and 5 positions, and comparisons with the spectra of **7** and **8**.

Excluding signals from the solvent CD_2Cl_2 and its impurities, there are 20 peaks in the δ = +90 to −50 ppm range that can be assigned to the $[V_4O_2(O_2CEt)_7(bpy)_2]^+$ cation; this is exactly the number expected for this cation with effective C_2 solution symmetry: 8 bpy resonances, 4 CH_3 resonances in a 2:2:2:1 relative integration ratio, and 8 CH_2 resonances in a 2:2:2:2:2:1:1 relative ratio resulting from the diastereotopic nature of each CH_2 pair of hydrogen atoms. These eight resonances occur in the δ = 30−90 ppm range as four pairs with comparable chemical shifts and T_1 times; the less intense pair at δ = 33.9

(40) Libby, E.; McCusker, J. K.; Schmitt, E. A.; Folting, K.; Hendrickson, D. N.; Christou, G. *Inorg. Chem.* **1991**, *30*, 3486.
(41) Shannon, R. D. *Acta Crystallogr. Sect. A* **1976**, *A32*, 751.

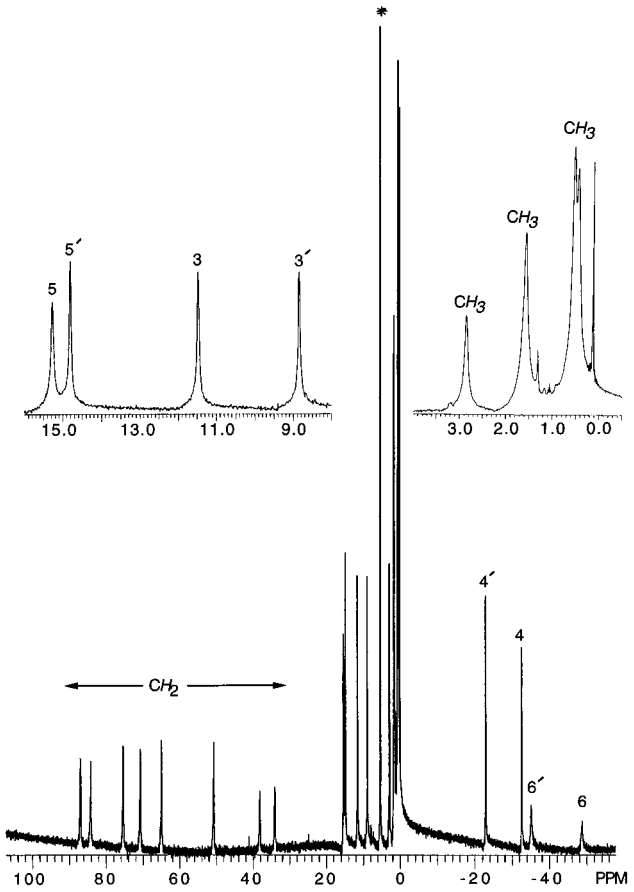

Figure 2. ^{1}H NMR spectrum of $[V_4O_2(O_2CEt)_7(bpy)_2](ClO_4)$ (**1**) in CD_2Cl_2 at ~23 °C. Primed and unprimed refer to the two halves of the bpy group. The peak marked with an asterisk is from solvent protio-impurities.

and 38.2 ppm is clearly from the unique $EtCO_2^-$ group bridging the body V atoms V(1) and V(2). The CH_3 resonances are less paramagneticallly shifted, as expected from their greater distance from the paramagnetic centers (paramagnetic shift α r^{-3}), and occur in the $\delta = 0-3$ ppm range, two only partially resolved; the integration value of the $\delta = 2.9$ resonance indicates it to be from the unique $EtCO_2^-$ group.

The assignment of the bpy resonances was facilitated by Me-substitution at the 4,4′ and 5,5′ positions (complexes **2** and **3**, respectively), which allowed identification of the resonances

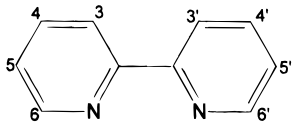

from the corresponding 4,4′ and 5,5′ hydrogen atoms as labeled in Figure 2; the other resonance positions did not differ much between **1**, **2**, and **3**. The 6,6′ hydrogen atoms are the closest to the metal centers and consequently give the most paramagnetically broadened resonances at $\delta = -35.2$ and -48.7 ppm. The remaining resonances at $\delta = 11.3$ and 8.8 ppm are then assigned by elimination to the 3,3′ hydrogen atoms. The bpy resonances display the alternating-shift pattern characteristic of contact shifts resulting from spin delocalization onto the bpy ligand via a π-delocalization pathway.[42] Thus, the 3/3′ and 5/5′ hydrogen resonances are paramagnetically shifted downfield, while the 4/4′ and 6/6′ pairs are shifted upfield. A π spin delocalization mechanism is consistent with unpaired spin only in d_π orbitals of near octahedral V^{III} and their overlap with the π system of the bpy rings. This mechanism is also supported by the change in sign of the isotropic shifts of the 4/4′ or 5/5′ Me groups compared with the shifts of hydrogens at these positions (Table 4).

Table 4. ^{1}H NMR Spectral Data[e] for $[V_4O_2(O_2CEt)_7(L-L)_2]^{+,-}$ (L−L = bpy, pic^-) Complexes

	1	**2**	**3**	**5** [f]
CH_2	86.7, 70.7[a]	85.6, 69.6	87.3, 69.1	74.4, 64.6
	84.0, 50.7[b]	83.1, 49.3	82.1, 47.9	69.7, 42.3
	75.2, 64.9[c]	74.0, 63.8	74.7, 62.3	66.3, 49.4
	38.2, 33.9[d]	37.3, 33.3	51.9, 33.6	30.7
CH_3	2.9[d]	3.2	3.3	2.3
	1.6[a]	1.4	1.5	1.3
	0.6[c]	1.0 (br)	1.1	0.5
	0.5[b]		1.0	0.4
3/3′	11.3, 8.8	10.4, 8.0	10.5, 8.0	16.3
4/4′	−32.7, −22.9	(47.2, 34.1)[g]	−21.7, −31.5	−27.5
5/5′	15.1, 14.7	15.3, 14.8	(−5.8, −10.9)[g]	18.6
6/6′	−48.7, −35.2	−34.1, −47.7	−36.1, −49.1	−47.5

[a−d] Superscripts identify the CH_2/CH_3 pairings deduced from the 2D spectra. [e] ~23 °C; in CD_2Cl_2 (**1**−**3**) or $(CD_3)_2CO$ (**5**); values are chemical shift from TMS using the δ scale (downfield shifts are positive). [f] Excluding small peaks assigned to the anti isomer. [g] Values in parentheses are for Me groups at these positions.

The spectrum of **5** in $(CD_3)_2CO$ comprises 17 peaks (Table 4). Seven peaks of equivalent intensity were found for the CH_2 groups between 30 and 75 ppm, similar to the 30−90 ppm region in Figure 2. The absence of an eighth resonance in the methylene region can be explained by the equivalent integration of the seven peaks; coincidental overlap of the two resonances for the unique bridging carboxylate (which would otherwise be half the intensity of the wingtip-body propionate methylene resonances) would account for the eighth methylene proton. Four peaks were found significantly shifted from the diamagnetic region; two upfield and two downfield; these resonances were assigned to the methyl protons of the propionate; there are also two resonances in a 2:3 ratio in the expected positions for the tetraethylammonium cation. These data are consistent with the anion being structurally similar to the cation of **1** with pic^- replacing the bpy groups. However, an additional 18−20 signals, all approximately 5% intensity relative to the major peaks of **5**, were also observed in the spectrum. It was first assumed that these were due to an impurity, but recrystallized material gave the same spectrum, with little change in the relative intensities, and the elemental analysis was consistent with the formula of **5**. We suspect that **5** occurs as a mixture of isomers. The two picolinate ligands can bind either syn or anti to each other (with respect to the orientation of the six-membered ring of picolinate). The syn configuration is observed in the crystal structures of $[M_4O_2(O_2CR)_7(pic)_2]^-$ (M = Cr,[43] Mn[40]) and is the most likely configuration for the major component of **5**. The anti isomer is observed in the neutral complex $[Mn_4O_2(O_2CPh)_6(pic)_2(MeCN)_2]$.[44] The large number of small additional peaks is consistent with an anti isomer (of lower symmetry than the C_2 syn isomer), and it is reasonable that the cause of the extra peaks should somehow involve the pic^- groups, since there is no evidence of an additional species in the spectra of **1**, **2**, or **3**.

***T_1* and 2D COSY Experiments.** With the exception of the resonances for the unique body−body bridging carboxylate

(42) *NMR of Paramagnetic Molecules*; La Mar, G. N., Horrocks, W. DeW., Jr., Holm, R. H., Eds.; Academic Press: New York, 1973.
(43) Donald, S.; Terrell, K.; Vincent, J. B.; Robinson, K. D. *Polyhedron* **1995**, *14*, 971.
(44) Libby, E.; Folting, K.; Huffman, C. J.; Huffman, J. C.; Christou, G. *Inorg. Chem.* **1993**, *32*, 2549.

Table 5. T_1 Relaxation Times for the Propionate Hydrogen Nuclei of Complex **1**

chemical shift (ppm)	T_1 (ms)	chemical shift (ppm)	T_1 (ms)
	CH_2		
86.7	10.4(3)	64.9	12.0(2)
84.0	10.4(3)	50.7	11.0(2)
75.2	12.4(3)	38.2	9.9(6)
70.7	10.6(2)	33.9	10.7(3)
	CH_3		
2.9	19.1(4)	0.6	21.4(9)
1.6	15.6(3)	0.5	18.5(3)

group, it was not possible to determine from the 1D ^{1}H NMR spectra which pairs of CH_2 resonances arise from protons bound to the same carbon or which CH_3 group is associated with which CH_2 protons. Because the longitudinal relaxation of a hydrogen nuclei is strongly influenced by its environment, even small changes in the hydrogen environment can have a substantial effect on the relaxation time (T_1). With this in mind, the T_1 times of each of the CH_2 and CH_3 resonances in **1** were measured. The measurements were made using a standard inversion−recovery pulse sequence[45] with a 90° pulse width of 10.4 μs. Calculation of the T_1 time was made using the exponential decay equation (eq 2), where M_z is the magnetization

$$M_z = M_0[1 - 2\exp(-\tau/T_1)] \quad (2)$$

in the z direction and τ is the delay between the 180° and 90° pulses. The results of the experiment are summarized in Table 5. It was hoped that the T_1 times would be different enough to allow pairs of diastereotopic protons to be assigned on the basis of similar T_1 times. This did not turn out to be the case, since the T_1 times for the CH_2 resonances were in a narrow range of 9.9(6)−12.4(3) ms and the CH_3 T_1 times in the range 15.6(3)−21.4(9) ms, precluding confident assignments. However, the desired assignments were achieved from a 2D COSY experiment. The broadness of the resonances and the large spectral window involved (160 ppm) caused some difficulties, but a satisfactory 2D spectrum was nevertheless obtained (Figure 3) with all the cross peaks visible. All cross peaks resulting from hydrogen nuclei in the same CH_2 group were clearly evident, allowing the eight CH_2 resonances to be assigned as the four pairings given in Table 4. In addition, cross peaks for the three-bond CH_2/CH_3 couplings were observed, as is better seen in the expanded view of Figure 4, leading to the CH_2CH_3 pairings of Table 4. Cross peaks for the protons of the bpy ligands were evident as well, and this allowed the resonances pertaining to each half of the bpy group to be grouped together: 11.3, −32.7, 15.1, −48.7 ppm (3, 4, 5, 6) and 8.8, −22.9, 14.7, −35.2 ppm (3′, 4′, 5′, 6′).

DC Magnetic Susceptibility Studies. Variable-temperature magnetic susceptibility studies were performed on powdered samples of complexes **1**, **5**, and **6** in the temperature range 2.00−320 K in a 10.0 kG (1T) applied magnetic field. The samples were restrained in Vaseline to prevent torquing. For complex **1**, the effective magnetic moment (μ_{eff}) per V_4 gradually rises from 5.79 μ_B at 300 K to a maximum of 6.80 μ_B at 25.0 K and then decreases rapidly to 4.72 μ_B at 2.00 K (Figure 5). The 300 K value is slightly higher than the spin-only ($g = 2$) value of 5.66 μ_B for a cation comprising four noninteracting V^{III} centers, suggesting the presence of some ferromagnetic exchange

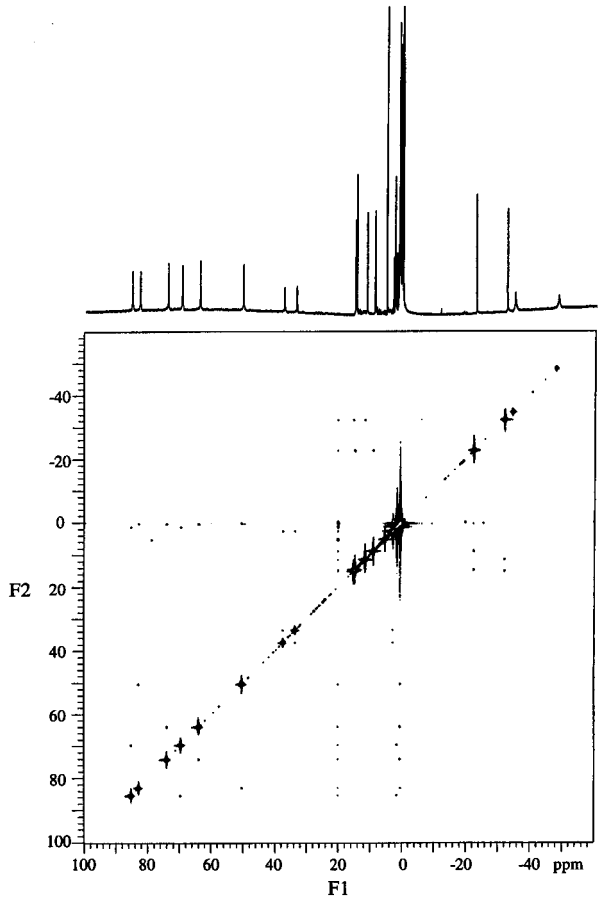

Figure 3. 2D COSY ^{1}H NMR spectrum of $[V_4O_2(O_2CEt)_7(bpy)_2](ClO_4)$ (**1**) in CD_2Cl_2. The vertical line of points at 20 ppm is an artifact that appears at the center of the spectral window.

interactions in **1**; the low-temperature values may be compared with the 4.90, 6.93, and 8.94 μ_B spin-only values expected for an exchange-coupled cation with a $S = 2$, 3, or 4 ground-state spin value, respectively.

The experimental μ_{eff} vs T data were fit to the theoretical expression derived previously[37,38,40] for a tetranuclear butterfly complex with C_{2v} symmetry, adjusted for the present case of $4V^{III}$ ($S = 1$) centers. This derivation using C_{2v} symmetry assumes all four body/wingtip interactions of the $[V_4O_2]^{8+}$ core are equivalent, and this simplifying and reasonable approximation allows application of the equivalent operator approach based on the Kambe vector coupling method.[46] The resulting spin Hamiltonian is given in eq 3, where J_{wb} is the wingtip/body

$$\hat{H} = -J_{wb}(\hat{S}_T^2 - \hat{S}_A^2 - \hat{S}_B^2) - J_{bb}(\hat{S}_A^2 - \hat{S}_1^2 - \hat{S}_3^2) \quad (3)$$

interaction, J_{bb} is the body/body interaction, $\hat{S}_A = \hat{S}_1 + \hat{S}_2$, $\hat{S}_B = \hat{S}_3 + \hat{S}_4$, and $\hat{S}_T = \hat{S}_A + \hat{S}_B$, where $\hat{S}_T$ is the resultant spin of the complete V_4 cation. The interaction between the two wingtip atoms V(3) and V(4) is assumed to be negligible, given their large separation (5.634(2) Å). The corresponding eigenvalue expression is given in eq 4 where constant terms have been ignored. In the present case of four V^{III} centers, $S_1 = S_2 = S_3 = S_4 = 1$, and there are a total of 19 spin states (S_T) with values ranging from 0−4.

$$E(S_T) = -J_{wb}[S_T(S_T + 1) - S_A(S_A + 1) - S_B(S_B + 1)] - J_{bb}[S_A(S_A + 1)] \quad (4)$$

A theoretical expression for the μ_{eff} vs T behavior of **1** was derived from the use of eq 4 and the Van Vleck equation; this

(45) Derome, A. *Modern NMR Techniques for Chemistry Research*; Pergamon Press: Oxford, 1987.
(46) Kambe, K. *J. Phys. Soc. Jpn.* **1950**, *5*, 48.

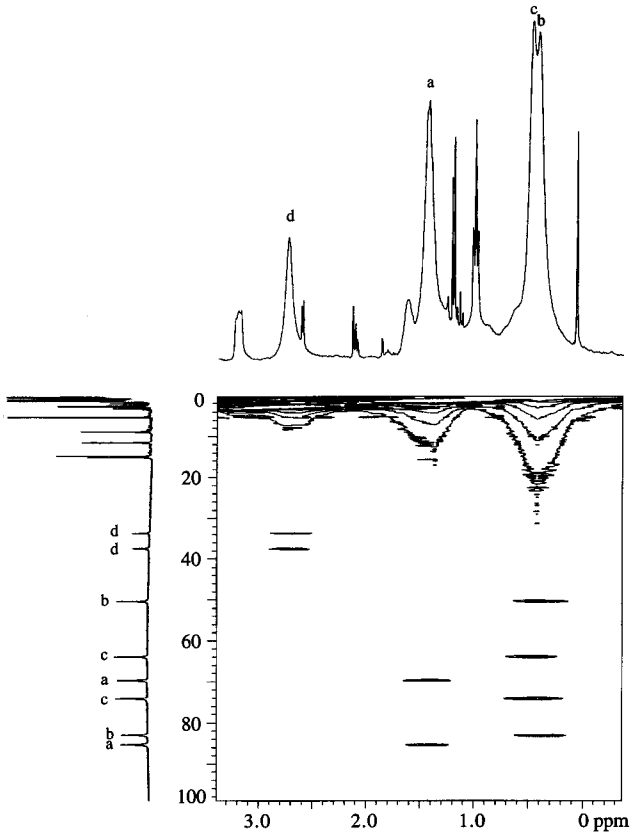

Figure 4. Expanded region of the 2D COSY ^{1}H NMR spectrum of complex **1** in CD_2Cl_2 showing CH_2/CH_3 cross peaks: CH_2/CH_3 pairings are indicated by the letters a−d.

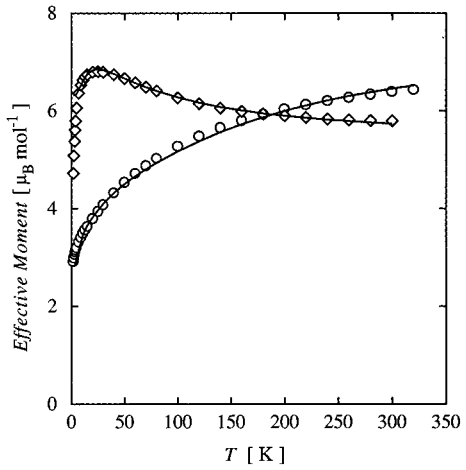

Figure 5. Plots of effective magnetic moment (μ_{eff}) per M_4 vs temperature for complexes **1** (◇) and **6** (○). The solid lines are fits to the appropriate expressions; see the text for the fitting parameters.

expression was then used to least-squares fit the experimental data measured in the 7.00−300 K range, and the fit is shown as a solid line on the μ_{eff} vs T plot in Figure 5. Data for temperatures below 7 K were omitted because the very rapid decrease in μ_{eff} is likely due primarily to zero field splitting (ZFS) effects within the ground-state spin manifold, and these effects were not incorporated into our fitting model. The fitting parameters were found to be $J_{bb} = -31.2$ cm^{-1}, $J_{wb} = +27.5$ cm^{-1}, and $g = 1.82$, with no correction term for paramagnetic impurities and a temperature-independent paramagnetism (TIP) term held constant at 400×10^{-6} cm^3 mol^{-1}. These values indicate that the ground state of complex **1** is, in the format (S_T,S_A,S_B), the (3,1,2) state, with a (4,2,2) first excited state and

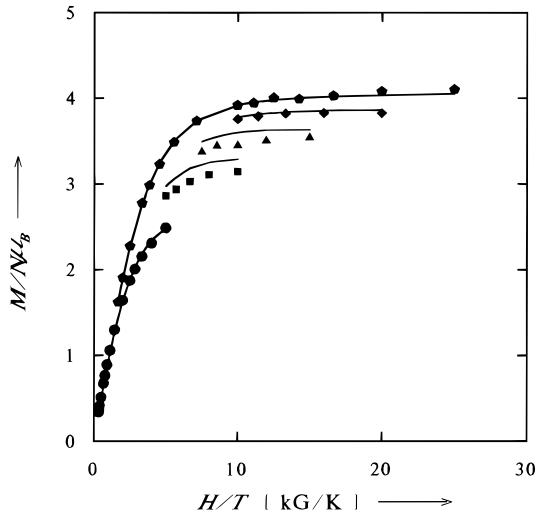

Figure 6. Plots of reduced magnetization ($M/N\mu_B$) vs H/T for complex **1** at 10 (●), 20 (■), 30 (▲), 40 (◆), and 50 (⬟) kG. The solid lines are fits to the appropriate expression; see the text for the fit parameters.

a triply degenerate second excited state, comprising the (2,0,2), (1,0,1), and (0,0,0) states, at energies above the ground state of 14.8 and 47.6 cm^{-1}, respectively. The low-lying $S_T = 4$ first excited-state rationalizes why the μ_{eff} vs T plot in Figure 5 rises to a maximum of 6.80 μ_B at 25.0 K, before decreasing to 6.36 μ_B at 7.00 K as the $S_T = 4$ first excited state is progressively depopulated and more of the molecules enter the $S_T = 3$ ground state. The μ_{eff} vs T data for complex **5** look similar to those shown in Figure 5 for complex **1**. Fitting of the data gave $J_{bb} = -31.2$ cm^{-1}, $J_{wb} = +27.0$ cm^{-1}, and $g = 1.85$. Complex **5** also has a $S_T = 3$ ground state.

For complex **6**, the μ_{eff} ($\chi_m T$) value per Cr_4 slowly decreases from 6.43 μ_B (5.17 cm^3 K mol^{-1}) at 320 K to 2.91 μ_B (1.06 cm^3 K mol^{-1}) at 2.00 K (Figure 5). The data were fit to the theoretical μ_{eff} vs T expression derived for a C_{2v} butterfly model (eqs 3 and 4) except that $S_1 = S_2 = S_3 = S_4 = 3/2$. The fitting parameters were found to be $J_{bb} = -19.4$ cm^{-1}, $J_{wb} = -11.2$ cm^{-1}, and $g = 1.99$, with no paramagnetic impurity term being required, and the TIP held constant at 400×10^{-6} cm^3 mol^{-1}. These values are very similar to those found for $[Cr_4O_2(O_2CMe)_7(bpy)_2](PF_6)$ by Bino, Pedersen, and co-workers using the same "two-J" model:[36] $J_{bb} = -25.5$ cm^{-1} and $J_{wb} = -15.7$ cm^{-1}, with g fixed at 1.98. The results for **6** indicate the ground state to be the (1,2,3) state with a low-lying (2,1,3) first excited state and a (0,3,3) second excited state at 12.2 and 26.7 cm^{-1}, respectively, above the ground state.

DC Magnetization vs Magnetic Field Studies. Confirmation of the ground-state spin value for complexes **1**, **5**, and **6** was sought by DC magnetization vs field studies employing applied magnetic fields (H) of 500 G to 50.0 kG in the 2.00−30.0 K temperature range. The data for complex **1** are shown in Figure 6 as reduced magnetization $M/N\mu_B$ vs H/T, where M is magnetization, N is Avogadro's number, and μ_B is the Bohr magneton. For a spin system populating only the ground state and exhibiting no ZFS effects, the various isofield lines should be superimposed and the $M/N\mu_B$ plots should saturate at gS_T, or approximately 6 for $g \approx 2$ and $S_T = 3$. Figure 6 shows that (i) the isofield lines are not superimposed, and (ii) the data at the highest field and lowest temperature saturate at $M/N\mu_B \approx 4$. Clearly, there is appreciable ZFS. The $M/N\mu_B$ vs H/T data were fit to a model that assumes that only the ground state is populated at the lowest temperatures and that includes Zeeman and axial ZFS (DS_z^2) interactions. A matrix diagonalization

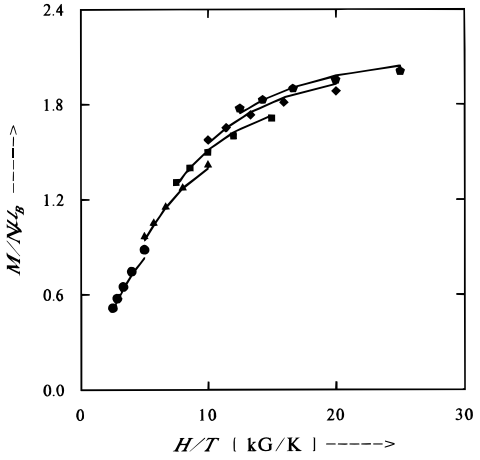

Figure 7. Plots of reduced magnetization ($M/N\mu_B$) vs H/T for complex **6** at 10 (●), 20 (▲), 30 (■), 40 (◆), and 50 (⬟) kG. The solid lines are fits to the appropriate expression; see the text for the fit parameters.

procedure described elsewhere was employed.[6] The solid lines in Figure 6 are the least-squares fits of the five isofield data sets plotted. Two different fits of the data were found, one with $D < 0$ and the other with $D > 0$; two minima are generally seen in the fitting of magnetization data. The fitting parameters for the fit shown as solid lines in Figure 6 are $S_T = 3$, $g = 1.93$, and $D = -1.52$ cm^{-1}. The other fit gave $S_T = 3$, $g = 1.96$, and $D = +3.55$ cm^{-1}. It is physically reasonable that $D < 0$ for a complex comprised of V^{III} ions. The D set of parameters is further supported by the AC susceptibility data (vide infra). The magnetization vs field studies thus confirm the conclusion from the χ_M vs T studies that complex **1** has a $S_T = 3$ ground state. The data for complex **5** (essentially identical with those for **1**) were similarly fit to give $S_T = 3$, $g = 2.00$, and $D = -1.50$ cm^{-1}.

For complex **6**, the $M/N\mu_B$ vs H/T data are shown in Figure 7, and comparison with Figure 6 shows two main differences: (i) the various isofield lines for **6** are more nearly superimposed than those for **1**, suggesting smaller ZFS in **6** vs **1**; and (ii) saturation of the $M/N\mu_B$ plot is not quite achieved, even at the highest H/T values, although extrapolation suggests saturation near ~2, the gS_T value expected for a S_T system with $g \approx 2$. Fitting of the data as for **1** and **5** gave the solid lines in Figure 7 with $S_T = 1$, $D = -0.17$ cm^{-1}, and $g = 2.04$, confirming the $S_T = 1$ ground-state deduced from the χ_M vs T studies.

Origin of the Ground States of 1 and 6. We have in previous reports described how spin frustration within the butterfly like $[M_4O_2]^{8+}$ cores lead to $S = 3$ and $S = 0$ ground states for the M = Mn^{III} and Fe^{III} cases, respectively. By spin frustration is here meant the presence within appropriate metal topologies of competing exchange interactions of comparable magnitude that lead to prevention (frustration) of the preferred spin alignments.[47,48] As a result, spin frustration can often lead to ground-state spin values larger than expected from the nature of the exchange interactions (e.g., even when all are antiferromagnetic). For the present cases of **1** and **6**, it is clear that spin frustration effects are operative. For **1**, J_{wb} is positive and J_{bb} is negative, but it is clearly impossible for the spins of the body V atoms to be concomitantly aligned antiparallel to each other and parallel to the spins of the wingtip V atoms. The preferred spin alignments are consequently frustrated because neither J_{wb} nor J_{bb} is insignificant (relative to the other). The ground-state thus becomes sensitive to the relative magnitude of the competing exchange interactions, i.e., the J_{wb}/J_{bb} ratio.

Table 6. Comparison of Magnetic Parameters for $[M_4O_2(O_2CR)_7(bpy)_2]^+$ Complexes

	V(**1**)	Cr(**6**)	Mn(**7**)	Fe(**8**)
J_{wb}, cm^{-1}	+27.5	−11.2	−7.8	−45.5
J_{bb}, cm^{-1}	−31.2	−19.4	−23.5	−8.9
S_T	3	1	3	0
M_b-O-M_b, deg[a]	96.3(2)	94.0(1)	96.3(7)	95.0(2)
M_w-O-M_b, deg[a]	123.6(2)	124.8(1)	123.7(8)	123.9(3)
	131.2(2)	131.0(1)	130.2(9)	131.9(3)
$M_b\cdot\cdot M_b$, Å	2.909(2)	2.784(1)	2.848(5)	2.855(4)

[a] Averaged values.

The (S_T, S_A, S_B) values of the ground states of **1** and **6** have been identified above as (3,1,2) and (1,2,3), respectively, and this allows the spin alignments in the ground state to be depicted: for comparison, the previously determined alignments for the M = Mn^{III} (**7**)[37,40] and M = Fe^{III} (**8**)[38] cases are also

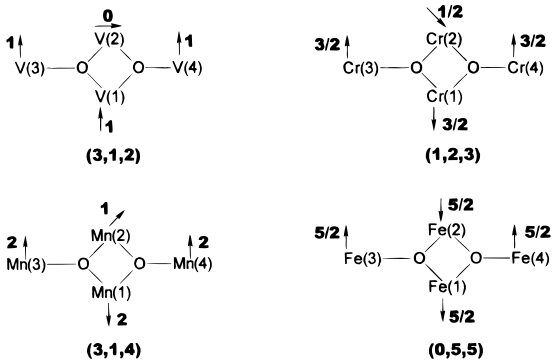

shown, and the same atom numbering scheme as Figure 1 is employed. The J_{wb} and J_{bb} values for **1**, **6**, **7**, and **8** are collected in Table 6. The body metal atoms are, of course, equivalent by symmetry and thus, for the V^{III}_4 complex, for example, this simple depiction is to be interpreted as indicating that the spins of V(1) and V(2) align neither perfectly parallel ($S_A = 2$) nor antiparallel ($S_A = 0$) but in an intermediate manner to give a resultant $S_A = 1$ which then aligns parallel to the $S_B = 2$ resultant to give the overall $S_T = 3$ ground state. The tendency of the body spins to align antiparallel (J_{bb} is negative) is opposed by the body-wingtip interaction (J_{wb}) which favors parallel alignment of spins. Thus, an intermediate situation is obtained, one that depends on the J_{wb}/J_{bb} ratio. Figure 8 shows the spin manifold as a function of J_{wb}/J_{bb}: For $0.5 < |J_{wb}/J_{bb}| < 1.0$, which includes the experimentally determined value for $|J_{wb}/J_{bb}|$ of 0.88, the ground state has $S_T = 3$ as depicted above. Note that even though J_{bb} (−31.2 cm^{-1}) is stronger than J_{wb} (+27.5 cm^{-1}), there is only one of the former and four of the latter; thus, the body spins are not aligned antiparallel, and J_{wb} primarily determines the ground state. For $|J_{wb}/J_{bb}| > 1.0$, however, the ability of the antiferromagnetic J_{bb} interaction to prevent perfectly parallel alignment of the body spins (as dictated by the ferromagnetic J_{wb}) is totally overcome, and all spins are parallel to give the $S_T = 4$ ground state. Similarly, for $|J_{wb}/J_{bb}| < 0.5$, the body spins are aligned antiparallel giving a triply degenerate ground state with $S_T = 0$, 1, and 2.

Similar considerations rationalize the ground state of the Cr^{III}_4 complex **6**. J_{wb} and J_{bb} are both antiferromagnetic, and the

(47) In accord with the suggestion by Kahn,[48] we shall employ terms such as "spin frustration degeneracy" for the special cases when competing exchange interactions lead to a degenerate ground state. Thus, we shall continue to employ the term "spin frustration" for the more general case where competing exchange interactions of comparable magnitude prevent (frustrate) the preferred spin alignments. This is in keeping with our practice to date, and with the most common meaning of the verb "to frustrate".

(48) Kahn, O. *Chem. Phys. Lett.* **1997**, *265*, 109.

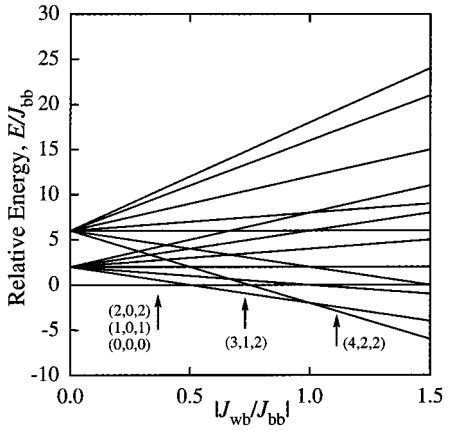

Figure 8. Plot of $|J_{wb}/J_{bb}|$ vs relative energy for the idealized C_{2v} symmetry core of $[V_4O_2(O_2CEt)_7(bpy)_2](ClO_4)$ (**1**) showing the change in ground state, indicated as (S_T, S_A, S_B).

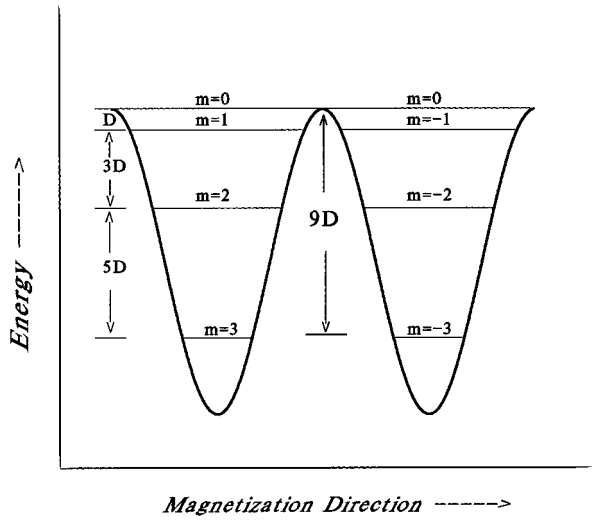

Figure 9. Double-well potential energy vs magnetization direction diagram for a $S_T = 3$ species with a negative ZFS parameter D. The thermal barrier for reversal of magnetization direction from $m_s = 3$ to $m_s = -3$ is $|9D|$.

system is frustrated. J_{bb} (-25.5 cm^{-1}) is stronger than J_{wb} (-15.7 cm^{-1}) but again, the greater number of the latter type causes the ground-state alignments to be dominated by J_{wb}, enforcing almost parallel alignment of the body spins to give the $S_T = 1$ ground state. An increase in the J_{wb}/J_{bb} ratio would give a $S_T = 0$ ground state, as seen for the Fe^{III}_4 complex, while a decrease in J_{wb}/J_{bb} would lead to a ground state with a higher S_T, as in the Mn^{III}_4 complex.

AC Magnetic Susceptibility Studies. Conclusive evidence that these $[V_4O_2]^{8+}$ complexes function as single-molecule magnets was obtained with AC magnetic susceptibility measurements. If, as indicated by one of two fits of the variable-field magnetization data, the $S_T = 3$ ground state of **1** and **5** experiences ZFS with $D = -1.5$ cm^{-1}, then the potential energy diagram in Figure 9 is applicable. This diagram is a plot of the potential energy of a single molecule vs the magnetization direction. The $S_T = 3$ ground state is split into $m_s = \pm3$, ±2, ±1, and 0 levels. In zero magnetic field and when $D < 0$, there are two states with the same lowest energy value, the $m_s = 3$ and $m_s = -3$ states. The $m_s = 3$ state can be viewed as the case where the magnetic moment of an individual molecule is "up" and the $m_s = -3$ state where the moment is "down". The double well shown in Figure 9 represents the change in potential energy as a single molecule converts from spin up to spin down by passing through the intermediate quantized levels. The potential-energy barrier is of height $|D|[\hat{S}_{z^2}|\pm3\rangle - \hat{S}_{z^2}|0\rangle] = 9|D|$. The barrier for complex **1** is calculated to be 9(1.52 cm^{-1}) = 13.68 cm^{-1}, if $D = -1.52$ cm^{-1}. Note that the other fit of magnetization data for complex **1** gave $D = 3.55$ cm^{-1}; a positive D value changes the diagram in Figure 9 such that the highest energy states are the $M_s = \pm3$ states. When D is positive, there is no potential-energy barrier to the reversal of the magnetization.

If a molecule has an appreciable barrier for reversal of the direction of its magnetic moment, then it can function as a SMM. Negative magnetic anisotropy ($D < 0$) and a relatively large spin ground state are required. As stated in the Introduction, in response to an external magnetic field, the magnetic moment of a SMM can be magnetized with its spin either "up" or "down" along the magnetic anisotropy axis; if the external field is now removed, the moment (spin) of the molecule will reorient only very slowly if the temperature is low. After saturation in a large field, the magnetization of $[Mn_{12}O_{12}(O_2CMe)_{16}(H_2O)_4]\cdot 2MeCO_2H\cdot 4H_2O$ relaxes with a half-life of greater than 2 months at 2K. There are several ways to determine if a molecule is a SMM. The most classic indication is a hysteresis loop in the plot of magnetization vs magnetic field. Several Mn_{12} complexes have been shown to exhibit magnetization hysteresis loops,[4−27] but none of the $[V_4O_2]^{8+}$ butterfly complexes show hysteresis effects in magnetization vs magnetic field data measured down to 1.70 K, the lowest limit of our SQUID magnetometer. However, a frequency-dependent out-of-phase AC magnetic susceptibility (χ''_M) signal is an equally good indicator that a molecule is a SMM. In the AC susceptibility experiment, the AC magnetic field is oscillated at a particular frequency, and a χ''_M signal is observed when the rate at which the magnetic moment of a molecule flips is close to this value. Thus, if a collection of SMMs are kept at a certain temperature and the frequency of the AC magnetic field is varied, a maximum in the χ''_M signal will occur when the frequency of the field equals the rate at which a molecule can interconvert between the two halves of the potential-energy double well shown in Figure 9. Frequency-dependent χ''_M signals have been reported for all of the known Mn_{12} SMMs.[4−27]

AC magnetic susceptibility data were collected for complexes **1** and **5**. Some of the data for $[V_4O_2(O_2CEt)_7(bpy)_2](ClO_4)$ (**1**) are shown in Figure 10. A polycrystalline sample was studied in the 1.7−30 K range with a 1.0 G AC field oscillating at either 250, 499, or 997 Hz. The DC magnetic field was held at zero. In the 10−30 K range, the value of $\chi'_M T$, where χ'_M is the in-phase AC susceptibility, remains constant at a value of 4.81 cm^3 K mol^{-1} (i.e., $\mu_{eff} = 6.20\ \mu_B$), consistent with a $S_T = 3$ ground state with $g = 1.82$. As can be seen in Figure 5, this AC value for $\chi'_M T$ is smaller than the $\mu_{eff} \approx 6.8\ \mu_B$ value in the 20−30 K range in a 10.0 kG DC field. The difference is likely due to the first excited state with $S_T = 4$ being partially populated in this temperature range in the presence of a 10.0 kG field, since this $S_T = 4$ state is only 14.8 cm^{-1} above the ground state.

At temperatures below 4.0 K, there are signs of slow magnetic relaxation for complex **1**. The value of $\chi'_M T$ decreases from 4.13 cm^3 K mol^{-1} at 4.0 K to 3.47 cm^3 K mol^{-1} at 1.7 K. This decrease could be due to an out-of-phase AC susceptibility signal (χ''_M), i.e., the temperature has been reduced to such a low value that the molecule cannot easily reverse the direction of its magnetization and therefore cannot keep in phase with the oscillating magnetic field. If so, a χ''_M signal should be seen. Indeed, complex **1** does exhibit a χ''_M signal at low temperatures

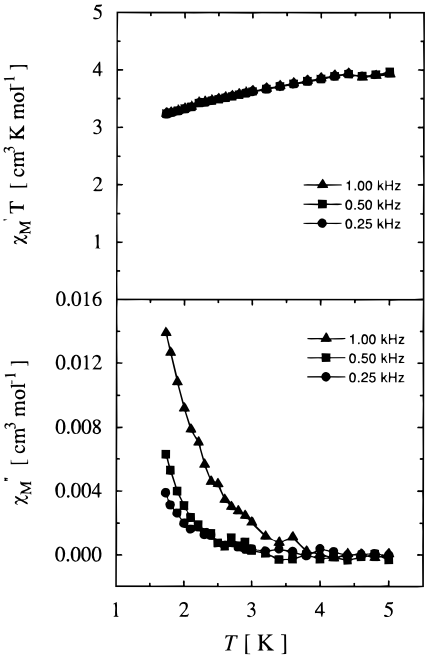

Figure 10. Plots of $\chi'_M T$ vs T (top) and χ''_M vs T (bottom) for $[V_4O_2(O_2CEt)_7(bpy)_2](ClO_4)$ (**1**) in a 1.0 G AC field oscillating at the indicated frequencies (and with no applied DC field), where χ'_M and χ''_M are the in-phase and out-of-phase magnetic susceptibilities, respectively.

(Figure 10), and, furthermore, it is frequency-dependent. However, the χ''_M signal is quite weak: at its maximum at the lowest accessible temperature of 1.70 K, it is only ~1−2% of the in-phase χ'_M signal.

Additional experiments were carried out to firmly establish that these $[V_4O_2]^{8+}$ complexes are SMMs. If they do indeed have the double-well potential shown in Figure 9, then the application of an external DC field would affect the temperature at which the χ''_M signal is seen.[16] The application of a DC field changes the double-well potential. An increase in the DC field leads to one-half of the double well becoming stabilized relative to the other half, i.e., the $m_s = -3$ level will be at lower energy than the $m_s = 3$ level. Furthermore, the barrier becomes larger as the DC field is increased. Thus, a DC field leads to the χ''_M AC peak moving to higher temperatures. The effect of an external DC field was examined for complexes **1** and **5**. It was found that the χ''_M signals for both complexes were shifted to higher temperature with an increasing DC field. The χ''_M signal for complex **1** became progressively larger with DC fields up to 10.0 kG, but it did not shift enough to show a peak in the χ''_M vs T curve. On the other hand, the χ''_M signal for the picolinate complex **5** did shift to high enough temperatures to show a peak in the χ''_M vs T plot (Figure 11). With the 1.0 G AC field oscillating at 1000 Hz, there is only a small frequency-dependent χ''_M signal seen when the DC field is zero, but an increase in the DC field to 1.0 kG leads to an increase in the magnitude of the χ''_M signal as the peak in the χ''_M vs T curve is presumably shifting to higher temperatures. Finally, when the DC field is 2.0 kG, there is a peak in the χ''_M vs T curve. Further increases in the DC field beyond 2.0 kG lead to a further shift to higher temperatures, until DC fields of ~5.0 kG, above which the temperature of the peak remains constant at ~2.2 K (Figure 12).

The frequency dependence of the χ''_M vs T peak for complex **5** was also studied. With the DC field held constant at 5.5 kG, an appreciable frequency dependence is seen (Figure 13). As the frequency of the AC field is changed from 1000 to 500 to 250 Hz, the peak in the χ''_M signal shifts from 2.2 to 2.0 to 1.7

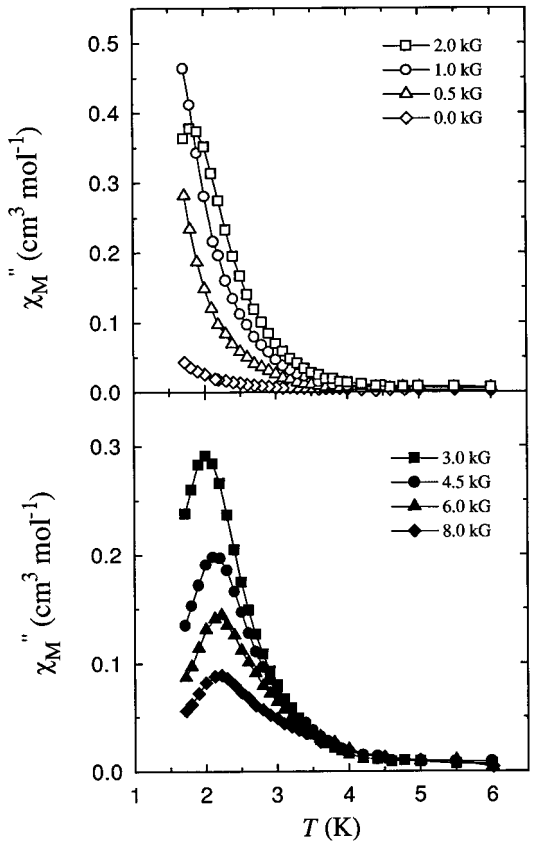

Figure 11. Plots of the out-of-phase AC susceptibility (χ''_M) vs T for $(NEt_4)[V_4O_2(O_2CEt)_7(pic)_2]$ (**5**) in a 1.0 G AC field oscillating at 1000 Hz and applied DC fields 0−2.0 kG (top) and 3.0−8.0 kG (bottom).

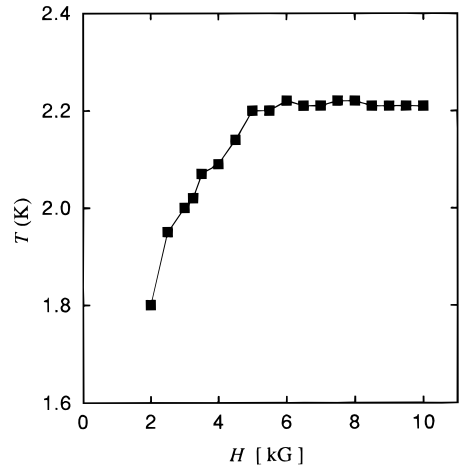

Figure 12. Variation of the temperature of the χ''_M peak maximum (in a 1.0 G AC field oscillating at 1000 Hz) as a function of applied DC field.

K. Further reduction to 50 Hz causes the χ''_M peak to shift to below 1.70 K. All of the above AC magnetic susceptibility data conclusively establish that complexes **5** and **1** function as SMMs. When magnetization vs magnetic field data are collected for these complexes at temperatures below 1.7 K, it is possible that a magnetization hysteresis loop may be observed.

It was noted that the peak in the χ''_M vs T data moved to temperatures > 1.7 K for complex **5** when the external DC field was increased, whereas the χ''_M vs T peak did not move above 1.7 K for complex **1**. This can be rationalized by reference to Figure 9. The barrier (U) for reversal of the magnetization direction is $U = |D|S^2$ for integer S, which is equal to $9|D|$ for

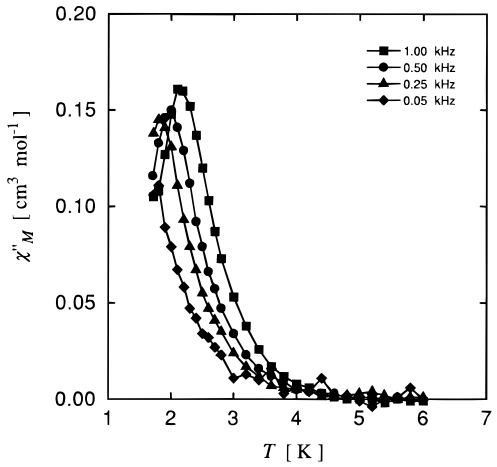

Figure 13. Plot of the out-of-phase AC susceptibility (χ''_M) vs T for $(NEt_4)[V_4O_2(O_2CEt)_7(pic)_2]$ (**5**) in a 1.0 G AC field oscillating at the indicated frequencies and with a 5.5 kG DC field.

a SMM with a $S = 3$ ground state. Thus, the barrier height depends on the magnitude of D. If **1** has a smaller value of $|D|$ than **5**, then it would have a smaller barrier, and it would consequently require a lower temperature for complex **1** to show slow magnetization relaxation. Thus, its χ''_M vs T peak would occur at a lower temperature than that for **5**. It is known that fitting variable-field magnetization data does not give a very precise determination of D; in the analysis of our data, we obtained comparable D values for complexes **1** and **5**. High-field EPR data are needed to get better determinations of D for these complexes.

Additional comments about the DC field dependence of the χ''_M AC peak temperature can be made. Since the barrier for magnetization reversal is ~13.5 cm^{-1} at temperatures below 3 K where χ''_M vs T peaks are seen for complex **5**, there is not nearly enough thermal energy to go over the barrier. Each complex must reverse its magnetization direction by quantum mechanically tunneling from one side of the double-well potential curve to the other side. The tunneling is due to the presence of a transverse magnetic field or zero-field interaction terms. The transverse magnetic field arises from a combination of the external magnetic field or an internal magnetic field from either the nuclear spins of the atoms or dipolar interactions between $[V_4O_2]^{8+}$ molecules. The rate of tunneling will vary as the magnitude of the external DC field is changed.[16] At zero DC field, the energy levels ($m_s = -3, -2, -1$) on the right-hand of the double well are aligned with those on the left side ($m_s = 3, 2, 1$), and the rate of tunneling is relatively large. This is termed "resonant magnetization tunneling". When a DC field is introduced, the energy levels on the two sides of the double well are not aligned, and the rate of tunneling will be less than when the DC field is zero. If the DC field is increased to a value that the $m_s = 3$ level lines up with the $m_s = -2$ level, then there would be another increase in the rate of tunneling. At this large field, the χ''_M vs T peak temperature would also decrease. Thus, the DC field dependence of the χ''_M vs T peak temperature shown in Figure 11 for complex **5** is understandable. There is a decrease at zero DC field, and the peak temperature is constant in the 5−10 kG range. If the DC field was increased to a value given by $\Delta H = |D|/g\mu_B$, then the $m_s = 3$ level would be aligned with the $m_s = -2$ level, and the χ''_M peak temperature would again show a decrease. However, it would require a field of ~17.0 kG to see this second dip in the χ''_M peak temperature, and unfortunately our AC SQUID used has a DC field limitation of 10.0 kG.

Concluding Comments

The described synthesis procedures provide convenient access to the new family of $[V_4O_2(O_2CR)_7(bpy)_2]^+$ (R = Et, Ph) species and certain Me-substituted bpy derivatives. Yields and purity are good, and the procedures involve readily available starting materials. X-ray crystallographic studies have confirmed that the representative complex **1** contains a butterfly $[V_4O_2]^{8+}$ core, making this the fourth member of the $[M_4O_2(O_2CR)_7(bpy)_2]^+$ series, which currently encompasses $M = V^{III}$, Cr^{III}, Mn^{III}, and Fe^{III}; it is possible that the series could be extended to include the, e.g., Ti^{III} and Co^{III} analogues, but this has yet to be explored. The structures of the four complexes are essentially superimposable.

DC magnetic susceptibility studies show that $[V_4O_2]^{8+}$ complex **1** has a $S_T = 3$ ground state and that, as might be expected from the differing electron counts involved, the four members of the $[M_4O_2]$ family have differing ground-state spins, i.e., $S_T = 3$ (V and Mn), 1 (Cr), or 0 (Fe). Both the $S_T = 3$ value for **1** and the variation in the M = V−Fe series can be readily rationalized using straightforward ideas of spin frustration arising from the particular combinations of magnitudes and signs of the exchange interactions present in the $[M_4O_2]^{8+}$ cores. This is particularly satisfying given the relatively large size and relatively low symmetry of these species.

AC magnetic susceptibility experiments, both with and without an external DC magnetic field, conclusively establish that these $[V_4O_2]^{8+}$ complexes are new examples of single-molecule magnets. The combination of a $S_T = 3$ ground state and a *negative* magnetoanisotropy associated with ZFS (DS_z^2), where $D \approx -1.5$ cm^{-1}, gives a large enough barrier ($U \approx 13.5$ cm^{-1}) to magnetization reversal that the complexes exhibit slow relaxation of magnetization. For comparison, the Mn_{12} SMMs have $S_T = 9$ or 10 ground states with $D \approx -0.5$ to -0.6 cm^{-1} and a barrier $U \approx 50$ cm^{-1}, giving out-of-phase AC susceptibility signals (χ''_M) in the 4−7 K ($S_T = 10$) or 2−4 K ($S_T = 9$) regions. The $[Mn_4O_3X]^{6+}$ distorted cubane complexes have $S_T = 9/2$, $D \approx -0.3$ to -0.4 cm^{-1}, and $U \approx 6-8$ cm^{-1} and exhibit χ''_M signals in the 2−3 K range.

The identification of new SMMs outside Mn and Fe chemistry is a significant development and augurs well for the future breadth and scope of this new phenomenon. The negative anisotropy of V^{III} and the $[V_4O_2]^{8+}$ complexes suggest that additional SMM examples may be found in this area of early transition metal chemistry as long as ground state spin values are also sufficiently large, as might result from spin frustration effects within appropriate V_x topologies. Also significant are the results of the 1D and 2D ^1H COSY NMR studies that establish that the complexes retain their structure on dissolution in CH_2Cl_2. Among the many advantages of SMMs over normal nanomagnets are single, sharply defined size and solubility, the latter having obvious benefits in future technological applications that might require, e.g., thin films. Confirming the retention of structural and therefore magnetic integrity on dissolution makes these potential applications feasible.

Acknowledgment. This work was supported by the National Science Foundation.

Supporting Information Available: Tables of X-ray data collection and structure solution details, fractional coordinates, thermal parameters, and interatomic distances and angles (14 pages). See any current masthead page for ordering information and Web access instructions.

JA9732439